Journal of Power Sources 269 (2014) 920–926

Contents lists available at ScienceDirect

Journal of Power Sources

journal homepage: www.elsevier.com/locate/jpowsour

Surface phenomena of high energy $Li(Ni_{1/3}Co_{1/3}Mn_{1/3})O_2$/graphite cells at high temperature and high cutoff voltages

Ting Liu [a], Arnd Garsuch [b], Frederick Chesneau [b], Brett L. Lucht [a, *]

[a] Department of Chemistry, University of Rhode Island, Kingston, RI 02881, USA
[b] BASF SE, GCN/EE – M311, 67056 Ludwigshafen, Germany

HIGHLIGHTS

- EIS suggests higher cathode impedance for cells cycled to higher potential.
- Ex-situ surface analysis used to investigate the surface of cycled electrodes.
- Thicker surface films are generated after cycling at higher working potential.

ARTICLE INFO

Article history:
Received 18 April 2014
Received in revised form
2 July 2014
Accepted 9 July 2014
Available online 19 July 2014

Keywords:
Lithium ion battery
Electrolyte
High voltage cathode
Ex-situ surface analysis

ABSTRACT

Layered $Li(Ni_{1/3}Co_{1/3}Mn_{1/3})O_2$ (NCM) materials have been investigated at high working potential and elevated temperature to correlate electrochemical performance with changes to the electrode interface. Graphite/NCM cells were cycled to either 4.2 or 4.5 V vs Li/Li^+ at room temperature (25 °C) followed by moderately elevated temperature (55 °C). Cells cycled to 4.2 and 4.5 V have similar capacity retention, but the cells cycled to 4.5 V have poorer first cycle efficiency, efficiency upon cycling at 55 °C, and greater increases in cell resistance. Surface analyses indicate thicker surface films on the cathode after cycling to 4.5 V, compared to cycling at a lower voltage of 4.2 V. The thicker surface film on the cathode is the result of electrolyte oxidation to generate poly(ethylene carbonate) and lithium alkyl carbonates. Electrochemical impedance spectroscopy of three-electrode cells reveals that the cathode dominates the cell impedance and the cathode impedance is much greater for cells cycled to 4.5 V than cells cycled to 4.2 V.

1. Introduction

Layered transition metal oxides have been widely investigated as cathode materials for lithium ion batteries. The initial cathode material utilized for lithium ion batteries was $LiCoO_2$. While $LiCoO_2$ has excellent electrochemical properties, the high cost and toxicity of Co has resulted in the development of related layered metal oxides with alternative transition metals, typically Ni and Mn, in partial replacement of Co [1]. A variety of cathode materials have been reported, with different stoichiometric ratios of transition metals [2–4]. One of the more commonly investigated materials is $LiNi_{1/3}Co_{1/3}Mn_{1/3}O_2$ (NCM) which has a good balance of electrochemical properties [4,5]. However, significant challenges still exist for applications which require extended calendar life performance, especially for graphite/NCM cells cycled above 4.2 V.

It is well known that a solid-electrolyte interphase (SEI) is generated on the surface of the graphitic anode during the first few charging cycles, but the SEI is transiently stable and can be damaged upon long term cycling or cycling at moderately elevated temperature [6–8]. In addition, reactions of the electrolyte with the surface of the cathode at elevated temperature (>45 °C) or high operating potential (>4.3 V), can lead to performance loss and significant impedance rise [6,9]. There has been significant interest in increasing the cutoff potential of NCM cathode materials in order to increase the capacity and nominal cell voltage and thus improve the energy density. However, cycling NCM cathodes to higher potential can lead to performance loss due to the poor structural stability of the layered metal oxides at higher potential and electrolyte oxidation at the cathode interface [10]. The effect of electrolyte decomposition and changes to the cathode surface film on NCM cathodes cycled to high potential (4.5 V) is not well understood.

The electrochemical performance of graphite/$Li(Ni_{1/3}Co_{1/3}Mn_{1/3})O_2$ cells cycled to different cutoff potentials (4.2 and 4.5 V)

* Corresponding author.
E-mail address: blucht@chm.uri.edu (B.L. Lucht).

http://dx.doi.org/10.1016/j.jpowsour.2014.07.051
0378-7753/

has been investigated by electrochemical cycling and electrochemical impedance spectroscopy (EIS). After cycling, ex-situ surface analysis of the electrodes using a combination of X-ray photoelectron spectroscopy (XPS), scanning electron microscopy (SEM), and attenuated total reflectance Fourier transform infrared (ATR-FTIR) spectroscopy has been conducted in an effort to understand the relationship between surface films and electrochemical performance. The results suggest that electrolyte oxidation on the cathode surface at high potential (4.5 V) is a significant contributor to performance fade.

2. Experimental

All electrodes were obtained from BASF SE, Ludwigshafen, Germany. Composite $Li(Ni_{1/3}Co_{1/3}Mn_{1/3})O_2$ electrodes on aluminum foil contain 93% active materials along with 3% conductive carbon and 4% polyvinylidene difluoride (PVDF). Composite graphite electrodes on copper current collector consist of 90% graphite (Conoco Phillips) with 3% super P carbon and 7% PVDF binder. A solution of 1.0 M $LiPF_6$ in mixture of ethylene carbonate (EC) and ethyl-methyl carbonate (EMC), 3:7 (v/v), is used as the electrolyte. Whatman glass microfiber membrane separators (GF/D type) are used. All 2032 coin cells were built in an argon-filled glovebox and cycled on an Arbin Instruments battery cycler with a constant current – constant voltage protocol. Five formation cycles (1 cycle at C/20 rate, 2 cycles at C/10 rate, and 2 cycles at C/5 rate) were employed and presented with cycling data. After formation cycles, all cells were cycled at room temperature (25 °C) for 15 cycles at C/5 rate, followed by 30 cycles at high temperature (55 °C) at the same C/5 rate. Multiple cells were built with good reproducibility. Only the representative data is shown. Internal ohmic resistance was measured with respect to each cycle index after discharging on the Arbin battery cycler, applying a 100 μs, 100 mA current pulse. The resistance value is calculated by dividing the voltage difference during the pulse by the applied current, and averaged over continuous ten pulses.

A set of three-electrode cells were built for EIS experiments to clarify the individual contribution of impedance from cathode and anode electrodes. A lithium reference electrode is placed in between the NCM cathode and the graphite anode, separated by one layer of Whatman glassfiber separator and one layer of polypropylene/polyethylene (Celgard 2325) separator. EIS spectra were measured at full state of charge on a Solartron SI 1287 electrochemical interface and SI 1252 A frequency response analyzer, with an AC oscillation of 10 mV amplitude over the frequency range from 300 kHz to 0.02 Hz. Before each measurement, the cell was charged to 4.2 V or 4.5 V at a constant current followed by holding at a constant voltage for 10 h. Then the EIS was measured at the 6th, 21st, and 51st charging steps. EIS measurements on cathode (cathode vs. reference) and anode (anode vs. reference) were successively carried out after measurements of the full cell (cathode vs. anode).

Cells were disassembled after cycling at 55 °C. Harvested electrodes were rinsed with dimethyl carbonate (DMC) three times to remove residual electrolyte, and dried under vacuum overnight at room temperature. Samples were handled under Ar except for ~10 s during transfer from transfer vessel into the instrument chambers followed by evacuation or Ar purging. All XPS spectra were acquired with a PHI5500 system using Al Kα radiation (hν = 1486.6 eV) under ultra-high vacuum, and processed by Multipak 6.1 A software and XPS peak software (version 4.1). SEM images were collected on a JEOL 5900 scanning electron microscope. ATR-FTIR spectra were measured on Bruker Tensor 27 instrument in argon atmosphere.

3. Results and discussion

3.1. Cycling performance

Fig. 1a shows the specific discharge capacities of graphite/NCM cells cycled at cutoff voltages of 4.2 and 4.5 V Fig. 1b shows the coulombic efficiencies calculated for each cycle. When the cutoff voltage is 4.5 V, the initial discharge capacity is much larger than that obtained at 4.2 V, 187 versus 147 mAh g^{-1} for the first C/20 formation cycle. After 15 cycles at 25 °C, the capacities drop to 174 and 138 mAh g^{-1} for 4.5 and 4.2 V, respectively. By the end of 30 cycles at 55 °C, the capacities decrease to 135 and 91 mAh g^{-1}, respectively. Based on the capacity at the end of formation cycling, the capacity retention after cycling at 25 °C is 98% for cells cycled to both 4.2 and 4.5 V, while the capacity retention after cycling at 55 °C is 76% and 65%, for the cells cycled to 4.2 and 4.5 V, respectively. The first cycle efficiency is worse for the cell cycled to 4.5 V, 60%, than the cell cycled to 4.2 V, 88%. This irreversible capacity loss on the first formation cycle is largely due to the formation of the anode SEI from electrolyte decomposition [11], although the lower

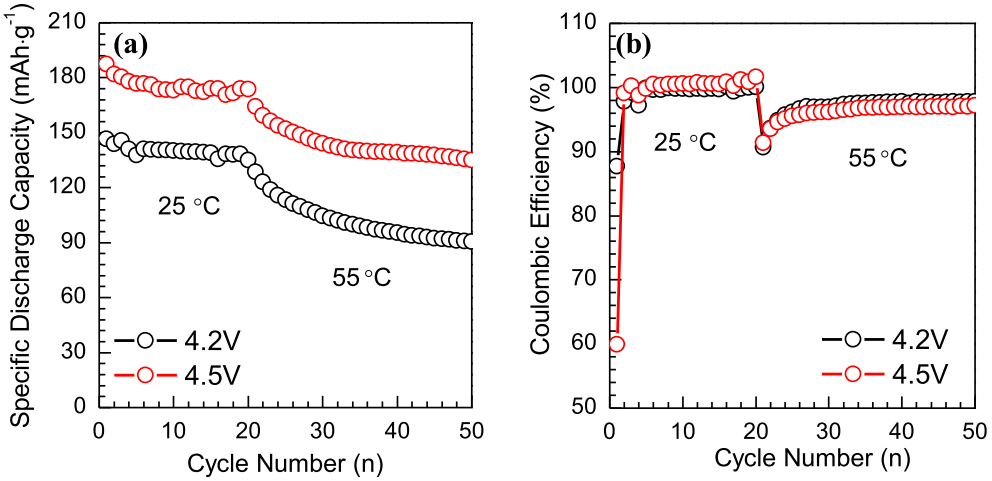

Fig. 1. (a) Specific discharge capacity and (b) coulombic efficiency of the NCM/graphite cells charged to two different cutoff voltages of 4.2 and 4.5 V, respectively. Formation cycles are also shown as the initial five data points.

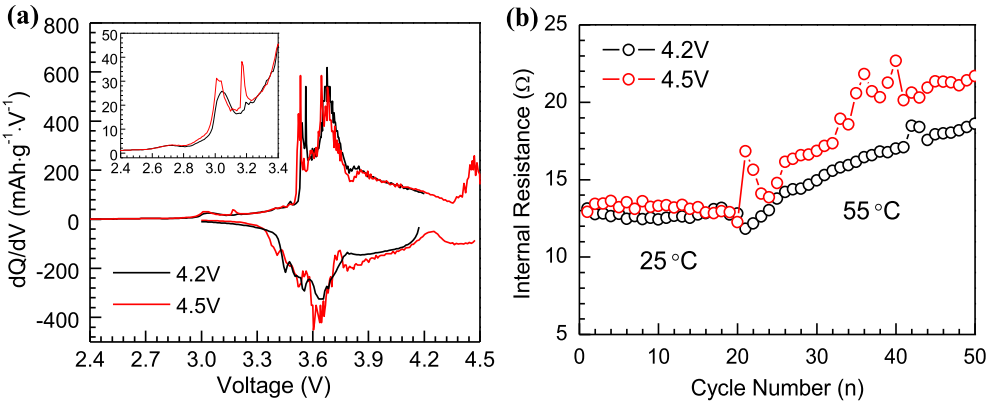

Fig. 2. (a) Differential capacity plots of the first formation (charging) cycle with cutoff voltages of 4.2 V and 4.5 V; inset: enlarged region of 2.4 V–3.4 V. (b) Internal resistance of the cells cycled at different voltages, which are measured after each discharge step.

efficiency for the cell cycled to 4.5 V is consistent with additional electrolyte decomposition on the cathode surface.

The difference in first cycle efficiency correlates well with the differential capacity curves as shown in Fig. 2a. The two reaction peaks at 3.0 and 3.2 V result from the decomposition of $LiPF_6$ electrolyte. In addition to the oxidation peaks at 3.5–3.8 V, which are attributed to the Ni^{2+}/Ni^{4+} couple [12], a peak is observed at 4.45 V which is assigned to electrolyte oxidation at the cathode surface which contributes to the lower first cycle efficiency. The oxidation of EC has previously been reported to result in the generation of polyethylene carbonate on the cathode surface [1] as part of the cathode-electrolyte-interface (CEI). Fig. 2b shows the internal resistance measured after each discharge cycle. Cycling at room temperature, both cells have stable resistance values. However, the resistance increases and efficiency decreases at both cutoff potentials upon cycling at 55 °C, due to further degradation of electrolyte and deposition of more insulating components on the electrode surfaces [13]. The cell cycled at 4.5 V has a greater increase in resistance than the cell cycled at 4.2 V. Therefore, the thermal abuse has a larger impact when the working potential is higher.

3.2. AC impedance measurements

AC impedance measurements were conducted at a full state of charge after formation cycles, after 15 cycles at 25 °C, and after an additional 30 cycles at 55 °C in three-electrode coin cells to monitor electrochemical processes occurring at individual electrodes as well as in full cells as a function of cycle number and working potential. Nyquist plots are depicted in Fig. 3. The first semicircle at higher frequency range primarily arises from the resistance and capacitance of the surface layer on the anode (R_{SEI}) and cathode (R_{CEI}). The second semicircle in the middle to low frequency range comes from the charge-transfer resistance (R_{CT}) of the cells. The sloped line at low frequency corresponds to the Warburg diffusion impedance [14]. A few observations can be drawn from the results in Fig. 3. First, the cell cycled at 4.5 V has larger overall impedance than the cell cycled at 4.2 V, which correlates well the continuously increased internal resistance as discussed above. Second, the impedance of the full cells is dominated by the impedance of the cathode, which is consistent with previously reported results [15]. Third, while the impedance of the cathode increases considerably upon extended cycling at

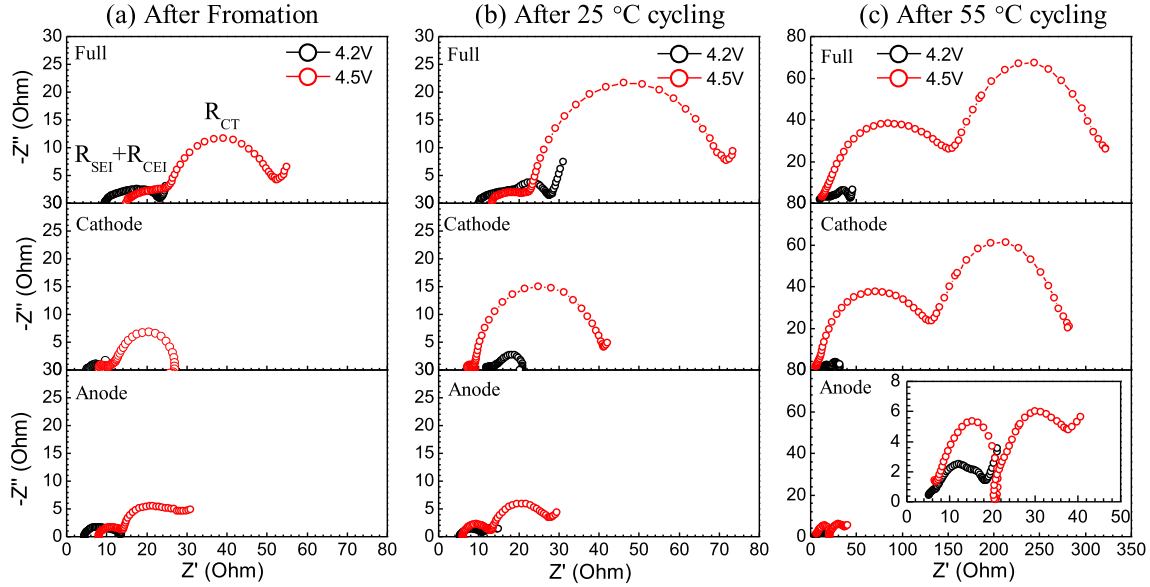

Fig. 3. Nyquist plots of NCM/graphite 3-electrode cells (a) after formation cycles, (b) after 25 °C cycles, and (c) after all 55 °C cycles, EIS spectra were collected at the cutoff voltages of 4.2 or 4.5 V. Inset: enlarged Z_{re} region of (0–50 Ω) on the anode electrodes after 55 °C cycles.

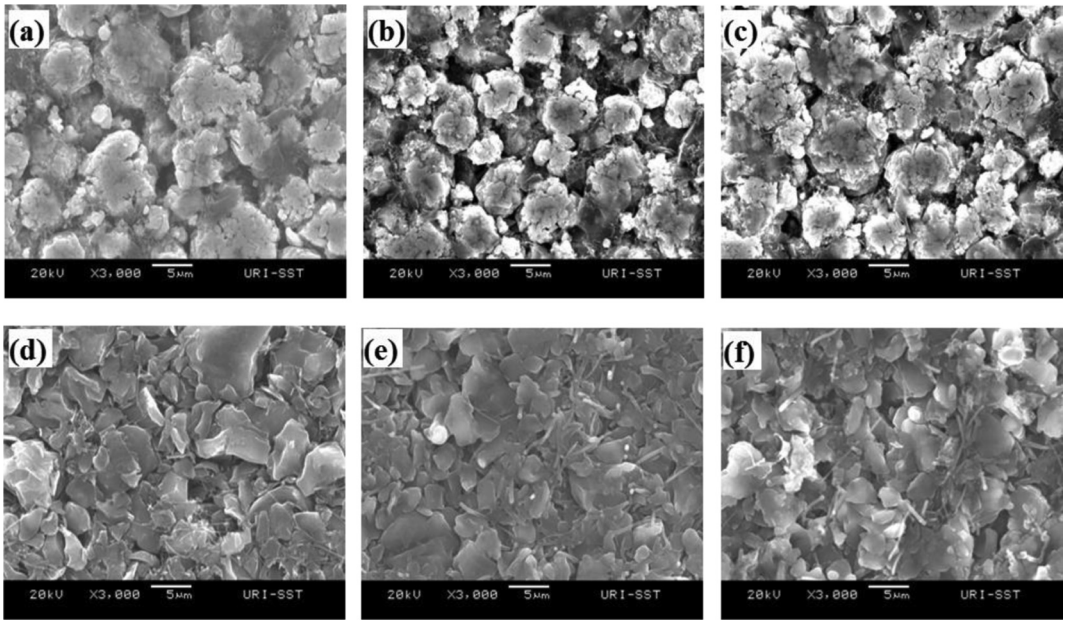

Fig. 4. SEM images of NCM cathodes (top row) and graphite anodes (bottom row) that are pristine (a, d), after cycling at 55 °C 4.2 V (b, e) and 4.5 V (c, f).

higher voltage, the impedance of the anode is only slightly increased, consistent with an evolution of the anode SEI. Fourth, the cell cycled to higher voltage has an increased R_{CT} on the cathode after 25 °C cycling, however, further cycling at 55 °C causes not only the growth in R_{CT}, but also the interfacial resistance of the cathode, R_{CEI}. Electrolyte decomposition on the cathode is enhanced at higher voltage and high temperature forming more resistive surface films, which is supported by ex-situ surface analysis discussed below. The electrolyte decomposition is also consistent with the lower coulombic efficiency at 55 °C observed in Fig. 1b.

3.3. Surface analysis

The SEM images of the fresh and cycled electrodes are depicted in Fig. 4. The morphologies of the NCM cathode materials after cycling to both 4.2 and 4.5 V have little evidence for change, consistent with stability of the bulk cathode materials under the cycling conditions. The edges of the graphitic anode particles are slightly dulled consistent with electrolyte decomposition to generate an SEI. However, there are no significant differences observed between the graphite anodes cycled to 4.2 or 4.5 V.

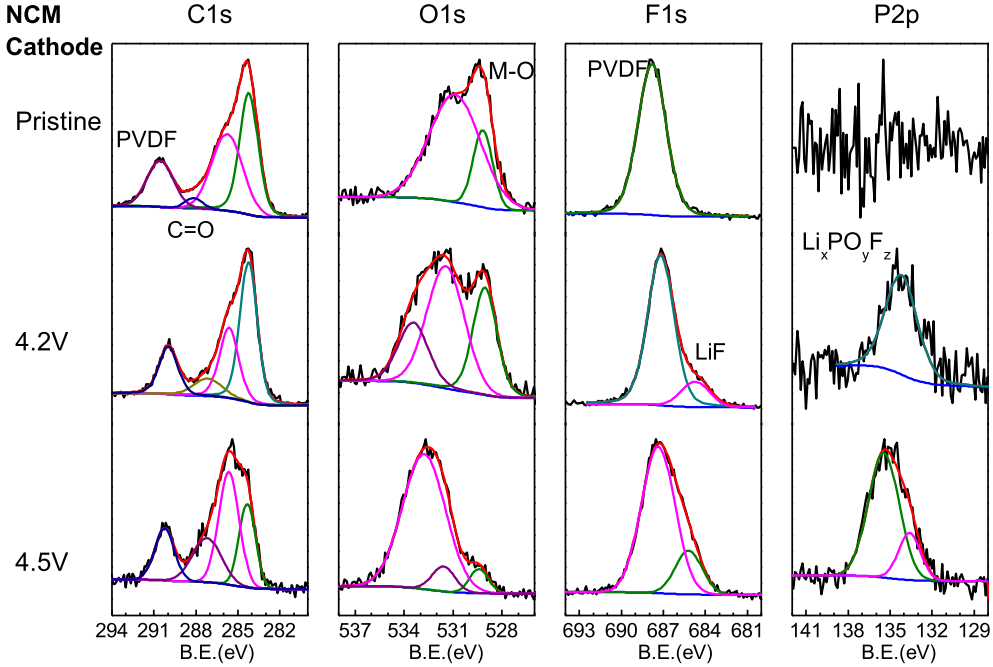

Fig. 5. C1s, O1s, F1s, P2p XPS spectra (black: experimental line; red: total fitting line; other colored line: individual fitting lines) of cycled NCM cathodes after 55 °C cycling, comparing to pristine cathode. (For interpretation of the references to colour in this figure legend, the reader is referred to the web version of this article.)

Table 1
Atomic concentrations of elements on electrode surfaces determined from XPS.

	Cathode				Anode			
	C	O	F	P	C	O	F	P
Pristine	62.7	13.3	24.0	0	76.2	11.2	12.6	0
4.2 V	55.9	17.4	25.5	1.2	40.1	22.8	30.5	6.6
4.5 V	41.8	21.2	30.7	6.3	31.3	31.6	29.6	7.5

To further investigate the effects of cutoff potential on electrode surface chemistry, XPS spectra were collected for all cycled electrodes. The XPS element spectra of the pristine and cycled NCM cathodes are provided in Fig. 5. The C1s spectrum of the fresh cathode contains a peak at 284.3 eV characteristic of conductive carbon and peaks at 285.8 and 290.2 eV for the PVDF binder. The O1s spectrum contains a peak characteristic of the bulk metal oxide at 529.2 eV and a broad peak at 531.5 eV characteristic of residual lithium carbonate [16]. The transition metal peaks (Ni, Co, and Mn) are weak and difficult to distinguish from the baseline. The F1s spectrum contains a single peak at 687.8 eV for the PVDF binder. Upon cycling, new peaks are observed on the surface of the NCM cathode particles consistent with electrolyte decomposition products. New peaks observed in C1s spectra at 286.5 and 288.5 eV are attributed to C–O and C=O containing species from electrolyte decomposition products including Li_2CO_3, lithium alkyl carbonates ($ROCO_2Li$), and polycarbonates [17]. Related peaks characteristic of C–O and C=O containing species are observed at 531.5–533 eV in O1s spectra. The F1s spectrum shows a new peak characteristic of LiF at 685 eV and a small peak is observed in the P2p spectrum at 134.5 eV indicating the presence of $Li_xPF_yO_z$ [18,19]. The intensity of the electrolyte decomposition products is greater for the electrodes cycled at 4.5 V than the electrodes cycled at 4.2 V. In particular, more salt decomposition in the form of $Li_xPF_yO_z$ (687 eV, F1s; 135 eV, P2p) appears to be observed on the surface of the cathode when cycled to 4.5 V. The slight shift in the P2p spectrum for electrodes cycled at higher potential may be due to high F content of the $Li_xPF_yO_z$. In addition, the peak characteristic of the metal oxide is significantly diminished for the electrode cycled at 4.5 V consistent with the generation of a thicker surface film on the cathode. The results suggest that there are more organic carbonate and $LiPF_6$ decomposition products on the cathode surface when the cell is cycled at higher potential. The changes to the elemental concentrations provide additional support (Table 1). The concentrations of O, F, and P are increased after cycling, especially at 4.5 V, while the concentration of C is decreased consistent with the deposition of more electrolyte decomposition products [20,21].

The XPS spectra of the pristine and cycled graphite anodes are provided in Fig. 6. The C1s spectrum of the fresh anode contains a peak at 284.3 eV for graphite and peaks at 285.8 and 290.2 eV for the PVDF binder. The corresponding F1s peak for PVDF is observed at 687.8 eV. A peak is observed at 532 eV in the O1s spectrum consistent with the presence of oxygenated impurities on the graphite surface. Upon cycling to either 4.2 or 4.5 V, changes are observed to the XPS spectra consistent with the formation of an anode SEI. New peaks are observed in the C1s spectrum at 286.5 and 288.5 eV characteristic of C–O and C=O containing species, respectively, while the corresponding O1s peaks are observed at 531.5–533 eV, respectively. The changes to the C1s and O1s spectra are consistent with the generation of an SEI composed of Li_2CO_3 or $ROCO_2Li$, as previously reported [7]. Changes are also observed in the F1s and P2p spectra. A new peak characteristic of LiF is observed in the F1s spectrum at 685 eV while a peak is observed in the P2p spectrum at 134.5 eV for $Li_xPF_yO_z$. The changes to the elemental concentrations provide additional support for SEI formation. The concentration of C is decreased while the concentrations of O, F, and P are increased. However, unlike the observations on the cathode, the differences in the XPS spectra for the anodes cycled to 4.2 and 4.5 V are small suggesting that the increase in potential does not have a large effect on the anode SEI.

FTIR spectra of the cathodes are provided in Fig. 7. Absorptions are observed at 1400, 1175 and 880 cm^{-1} for the fresh cathode and are attributed to the PVDF binder. After cycling at

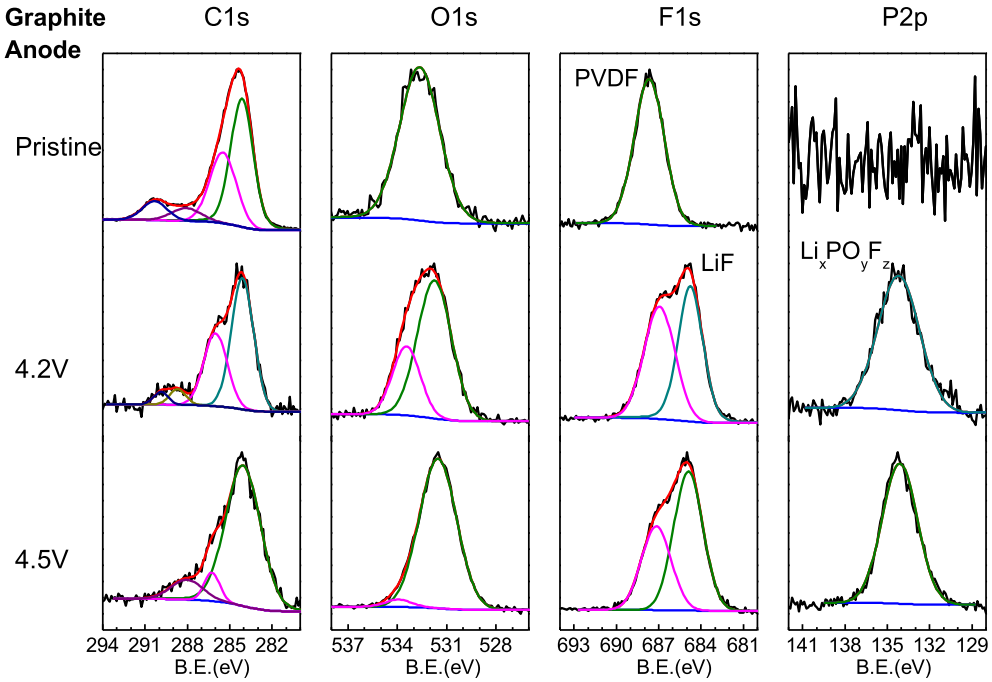

Fig. 6. C1s, O1s, F1s, P2p XPS spectra (black: experimental line; red: total fitting line; other colored line: individual fitting lines) of cycled graphite anodes after 55 °C cycling, comparing to pristine anode. (For interpretation of the references to colour in this figure legend, the reader is referred to the web version of this article.)

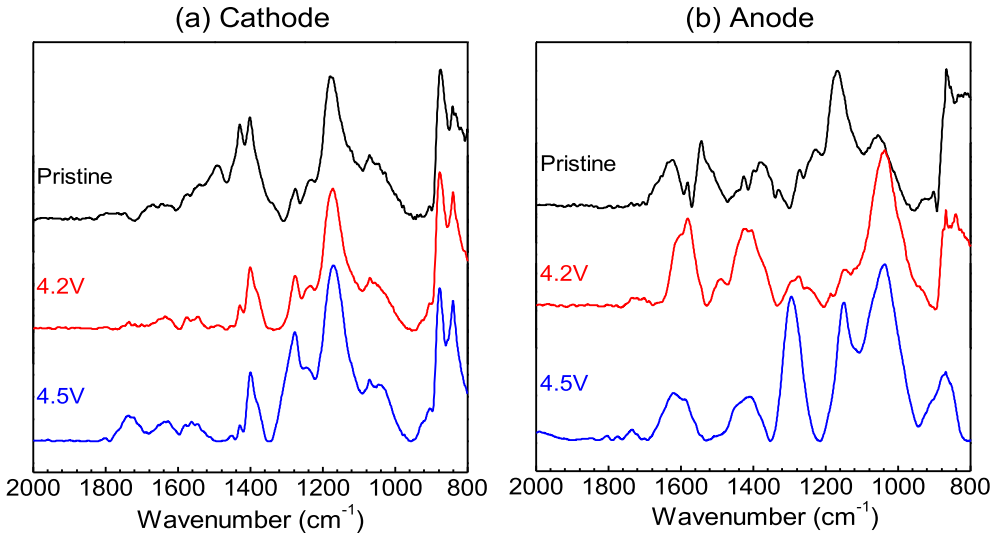

Fig. 7. FTIR spectra of electrodes cycled at 55 °C (a) NCM cathodes and (b) graphite anodes at different cutoff voltages. Pristine electrodes are also shown as black lines for comparison.

4.2 V there are only small changes to the IR spectrum of the cathode. The spectrum is dominated by the absorptions of PVDF. However, upon cycling to 4.5 V the changes to the cathode surface are more apparent. New absorptions are observed at 1640 and 1740 cm^{-1} characteristic of lithium ethylene dicarbonate (LEDC) and poly(ethylene carbonate), respectively [22]. The presence of additional electrolyte decomposition on the cathode after cycling to 4.5 V is in agreement with the differential capacity, EIS and XPS analysis.

The IR spectrum of the pristine anode is similar to the IR spectrum of the pristine cathode and is dominated by the PVDF binder. After cycling to 4.2 V new absorptions are observed at 1640, 1400, 1280, 1050 and 830 cm^{-1} characteristic of LEDC, as previously reported [23–25]. In addition, new absorptions observed at 1480 and 870 cm^{-1} are characteristic of Li_2CO_3 [24]. Thus, after cycling to 4.2 V, Li_2CO_3 and LEDC are dominant products observed on the anode surface, which is typical for carbonate based electrolytes [26] and consistent with the XPS results. After cycling at 4.5 V, the IR spectra are similar although the intensity of absorptions at 1295, 1150 and 910 cm^{-1} are increased. The new absorptions likely result from additional $Li_xPF_yO_z$ on the anode surface from additional $LiPF_6$ decomposition [11,27]. However, the changes to the anode are smaller than those observed on the cathode and in agreement with the EIS and XPS results.

4. Conclusions

Electrochemical cycling and ex-situ surface analysis of graphite/NCM cells cycled to different cutoff potentials, 4.2 and 4.5 V vs Li/Li^+, have been conducted. The cells have good capacity retention upon cycling to either cutoff potential, ~65–76% after total 50 cycles at 25 and 55 °C. However, the cells cycled to 4.5 V have poorer first cycle efficiency (60%) than the cells cycled to 4.2 V (88%) and a greater increase in impedance upon cycling at 55 °C. The lower first cycle efficiency and increased impedance suggest more electrolyte decomposition for cells cycled to 4.5 V. Ex-situ surface analysis by XPS and FTIR of the electrodes after cycling support additional electrolyte decomposition on the surface of cathodes cycled to 4.5 V. The cathode surface films include LEDC, poly(ethylene carbonate), LiF, and $Li_xPF_yO_z$. However, the oxidative ring opening of EC to generate poly(ethylene carbonate) (Equation (1)) is likely to be the most significant contributor to the impedance rise on the cathode [21]. Cycling graphite/NCM cells to 4.5 V, results in electrolyte oxidation on the cathode surface which contributes to performance loss.

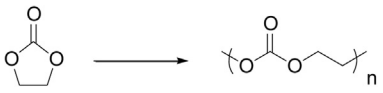

Eq. 1 (1)

A better understanding of the mechanism of performance fade for graphite/NCM can lead to the development of methods to improve performance. Since electrolyte oxidation on the cathode surface appears to be a significant contributor to capacity fade, the development of novel electrolytes which can inhibit electrolyte oxidation should lead to improved performance of graphite/NCM cells cycled to higher potential (4.5 V). Related cathode film forming additives have been shown to improve the performance of high voltage lithium- and manganese- rich layered-oxides (LMR-NMC) and $LiNi_{0.5}Mn_{1.5}O_4$ [28–31].

Acknowledgments

The authors thank BASF SE Scientific Network on Electrochemistry and Batteries for materials supply and financial support.

References

[1] D. Aurbach, K. Gamolsky, B. Markovsky, G. Salitra, Y. Gofer, U. Heider, R. Oesten, M. Schmidt, J. Electrochem. Soc. 147 (2000) 1322–1331.
[2] I. Saadoune, C. Delmas, J. Solid State Chem. 136 (1998) 8–15.
[3] Z. Lu, D.D. MacNeil, J.R. Dahn, Electrochem. Solid State Lett. 4 (2001) A200–A203.
[4] M.S. Whittingham, Chem. Rev. 104 (2004) 4271–4301.
[5] T. Ohzuku, Y. Makimura, Chem. Lett. 30 (2001) 642–643.
[6] M. Herstedt, D.P. Abraham, J.B. Kerr, K. Edström, Electrochim. Acta 49 (2004) 5097–5110.
[7] P. Verma, P. Maire, P. Novák, Electrochim. Acta 55 (2010) 6332–6341.
[8] S.S. Zhang, K. Xu, T.R. Jow, Electrochim. Acta 51 (2006) 1636–1640.
[9] X. Zhang, P.N. Ross, R. Kostecki, F. Kong, S. Sloop, J.B. Kerr, K. Striebel, E.J. Cairns, F. McLarnon, J. Electrochem. Soc. 148 (2001) A463–A470.
[10] G.H. Kim, J.H. Kim, S.T. Myung, C.S. Yoon, Y.K. Sun, J. Electrochem. Soc. 152 (2005) A1707–A1713.
[11] K. Xu, Chem. Rev. 104 (2004) 4303–4417.
[12] K.M. Shaju, G.V.S. Rao, B.V.R. Chowdari, Electrochim. Acta 48 (2002) 145–151.

[13] S.K. Martha, J. Nanda, G.M. Veith, N.J. Dudney, J. Power Sources 216 (2012) 179–186.
[14] S.S. Zhang, K. Xu, T.R. Jow, Electrochim. Acta 49 (2004) 1057–1061.
[15] D.P. Abraham, S.D. Poppen, A.N. Jansen, J. Liu, D.W. Dees, Electrochim. Acta 49 (2004) 4763–4775.
[16] L. Bodenes, R. Dedryvere, H. Martinez, F. Fischer, C. Tessier, J.P. Peres, J. Electrochem. Soc. 159 (2012) A1739–A1746.
[17] R. Dedryvere, S. Laruelle, S. Grugeon, L. Gireaud, J.M. Tarascon, D. Gonbeau, J. Electrochem. Soc. 152 (2005) A689–A696.
[18] L.E. Ouatani, R. Dedryvère, J.-B. Ledeuil, C. Siret, P. Biensan, J. Desbrières, D. Gonbeau, J. Power Sources 189 (2009) 72–80.
[19] M. Lu, H. Cheng, Y. Yang, Electrochim. Acta 53 (2008) 3539–3546.
[20] W. Li, B.L. Lucht, J. Electrochem. Soc. 153 (2006) A1617–A1625.
[21] Y. Shigematsu, S.-I. Kinoshita, M. Ue, J. Electrochem. Soc. 153 (2006) A2166–A2170.
[22] L. Yang, B. Ravdel, B.L. Lucht, Electrochem. Solid State Lett. 13 (2010) A95–A97.
[23] G.V. Zhuang, H. Yang, P.N. Ross, K. Xu, T.R. Jow, Electrochem. Solid State Lett. 9 (2006) A64–A68.
[24] S. Tsubouchi, Y. Domi, T. Doi, M. Ochida, H. Nakagawa, T. Yamanaka, T. Abe, Z. Ogumi, J. Electrochem. Soc. 159 (2012) A1786–A1790.
[25] M. Nie, D. Chalasani, D.P. Abraham, Y. Chen, A. Bose, B.L. Lucht, J. Phys. Chem. C. 117 (2013) 1257–1267.
[26] Y. Akita, M. Segawa, H. Munakata, K. Kanamura, J. Power Sources 239 (2013) 175–180.
[27] L.W. Daasch, D.C. Smith, Anal. Chem. 23 (1951) 853–868.
[28] L. Yang, B.L. Lucht, Electrochem. Solid State Lett. 12 (2009) A229–A231.
[29] L. Yang, T. Markmaitree, B.L. Lucht, J. Power Sources 196 (2011) 2251–2254.
[30] S. Dalavi, M. Xu, B. Knight, B.L. Lucht, Electrochem. Solid State Lett. 15 (2012) A28–A31.
[31] M. Xu, L. Zhou, Y. Dong, Y. Chen, A. Garsuch, B.L. Lucht, J. Electrochem. Soc. 160 (2013) A2005–A2013.